Effect of the doping element on the structure and UV–visible properties in the system Bi4V1.7(Si,Me)0.3O11-δ (Me = Si, P, Cu, and Co)

Abdelmajid Agnaou, Wafaa Mhaira, Rachida Essalim, Maati Alga, Mohamed Zamama, Fabrice Mauvy, Abdelaziz Ammar

Effect of the doping element on the structure and UV–visible properties in the system $Bi_4V_{1.7}(Si, Me)_{0.3}O_{11-\delta}$ (Me = Si, P, Cu and Co)

A. Agnaou [a*], W. Mhaira [a], R. Essalim [a], M. Alga [a], M. Zamama [a], F. Mauvy [b], and A. Ammar [a]

[a] *Laboratory of Materials Science and Process Optimization (SCIMATOP), Cadi Ayyad University, Faculty of Science-Semlalia, Av. My Abdellah, B.P. 2390, Marrakech, Morocco*

[b] *CNRS, Université de Bordeaux, (ICMCB), UMR 5026, 87, Av. Dr A. Schweitzer, 33608, Pessac, France*

** Corresponding author. E-mail address: agnaouabdelmajid@gmail.com (A. Agnaou)*

Abstract

While BIMEVOX systems have attracted the attention of researchers for their electrical conductivity by O^{2-} oxide ions at relatively low temperatures, there is only a limited number of works concerning their local structure. In this work, the $Bi_4V_{1.7}(Si.Me)_{0.3}O_{11-\delta}$ (Me = Si, P, Cu, and Co) system is studied using X-ray powder diffraction (XRD), Raman spectroscopy, IR spectroscopy, SEM-EDX, UV-visible spectrophotometry, and differential scanning calorimetry (DSC). The three main polymorphs α, β, and γ are obtained at room temperature. In the case of the $Bi_4Si_{0.15}P_{0.15}V_{1.70}O_{11-\delta}$ compound, two successive structural transitions were observed, while only one structural transition was observed for the $Bi_4Si_{0.30}V_{1.70}O_{11-\delta}$ compound. The UV-Vis Diffuse reflectance spectroscopy (DRS) indicates that the double-doped $Bi_4V_{1.7}(Si.Me)_{0.3}O_{11-\delta}$ compounds present a band gap energy in the range $1.76 \leq Eg \leq 2.36$ eV and $Bi_4Si_{0.15}Co_{0.15}V_{1.70}O_{11-\delta}$ presents the narrowest band gap.

Keywords: BISIMEVOX.15, XRD, DSC, SEM, UV-visible.

1. Introduction

Research on the binary Bi_2O_3-V_2O_5 allowed us to highlight, at the end of the 80s, the compound $Bi_4V_2O_{11}$ [1]. This oxide has a remarkably high O^{2-} ion conductivity and can be used as the electrolyte in oxygen sensors, oxygen separation systems, and solid oxide fuel cells [2–5].

$Bi_4V_2O_{11}$ is a member of the Aurivillius $2(Bi_2O_2)^{2+}(A_{n-1}B_nO_{3n+1})^{2-}$ family compounds, whose structure consists of alternating fluorite-like $(Bi_2O_2)^{2+}$ layers and perovskite-like $(A_{n-1}B_nO_{3n+1})^{2-}$ blocks. In the case of $Bi_4V_2O_{11}$ (n=1), the perovskite-like layers are reduced to a layer of oxygen-deficient octahedra $(VO_{3.5}\square_{0.5})^{2-}$ [6].

The presence of oxygen vacancies and the non-bonding electronic pair of bismuth (III), allowed $Bi_4V_2O_{11}$ to acquire a high electrical conductivity explained by the high mobility of O^{2-} ions. Furthermore, the compound $Bi_4V_2O_{11}$ exhibits, as a function of temperature, three crystal phases α-monoclinic, β-orthorhombic, and γ-tetragonal. The description of the crystal lattices of

these polymorphs can be performed by means of an orthorhombic mean lattice of parameters: $a_m \approx 5.53$, $b_m \approx 5.61$, $c_m \approx 15.28$ Å [7], such that $a_\alpha = 3a_m$, $b_\alpha = b_m$, $c_\alpha = c_m$; $a_\beta = 2\,a_m$, $b_\beta = b_m$, $c_\beta = c_m$, and $a_\gamma = b_\gamma \approx a_m/\sqrt{2}$, $c_\gamma \approx c_m$. The α to β transition occurs around 430 °C upon heating. The transition $\beta \rightarrow \gamma$ occurs by the disappearance of the anionic vacancy order around 550 °C. Thus, the modulation lines related to the β-orthorhombic form disappear reversibly and the cell becomes of tetragonal symmetry, with the space group I4/mmm. The γ phase, obtained at high temperature, is the most disordered and therefore, the most conductive [8, 9]. The tetragonal phase is characterized by a total disorder of the oxygen vacancies, which corresponds to the statistical distribution of the vacancies around cations in the perovskite layers. This facilitates the migration of O^{2-} ions in these layers. However, the order of the anion vacancies leads to a superstructure with a doubling of the a parameter (β-phase) or a tripling of the a parameter (α-phase). This order affects the mobility of O^{2-} ions in these phases. The partial substitution of vanadium (V) by a cation (ME) allows the stabilization of the latter phase at low-temperature. Thus, the obtained $Bi_4V_{2-x}Me_xO_{11\pm\delta}$ solid solutions present, around 600 °C, electrical conductivities around 10^{-1}-10^{-2} S.cm^{-1} [3–6, 10]. These new materials are known by the acronym BIMEVOX, ME is the substituent cation. Depending on the degree of substitution of the vanadium, the nature of the doping element ME (ionic radii and covalence of the bond ME-O), and the rate of oxygen vacancies, the resulting phases can take the form of one of the three polymorphs α, β or γ. BIMEVOX materials are tested as solid electrolytes [11], oxygen separation membranes [2], potentiometric and amperometric gas sensors [12] and they are used as base materials for SOFC fuel cells (as electrolytes or anodes).

Moreover, as we know, the band structure of semiconductors is a fundamental element to develop the applications of photo-electrochemistry. The compound $Bi_4V_2O_{11}$ is a semiconductor that reacts to visible light. This oxide can absorb nearly 11 % of the sunlight due to its band gap higher than 2 eV. The band gap energy varies according to the authors: 2.86 eV [13], 2.08 eV [14], and 2.19 eV[15, 16]. Thus, doping this compound would produce intermediate energy levels in the band gap and improve the optical performance of this semiconductor. $Bi_4V_2O_{11}$ and some BIMEVOX materials were used as photoanodes for the first time by K. Trzciński et *al*. [17] and it has been shown that $Bi_4V_2O_{11}$ compound is a semiconductor with relatively narrow energy band gap E_g and that the substitution of vanadium by Cu, Zn and Mn causes a decrease in the E_g values. This property makes BIMEVOXes potentially attractive for application in photoelectrocatalysis.

We have shown in recent studies [10, 18, 19], that the electrical conductivity and the activation energy depend on the nature of the doping ion. We also found that the double substitution of vanadium in $Bi_4V_2O_{11}$ improves these properties in most of the studied phases.. The doping ions were chosen from the d and p blocks of the periodic table. Thus, it seemed

interesting to us to explore the effect, on energy band gap, of these double substitutions with elements of a different nature, which, allowed the stabilization of the different polymorphs of $Bi_4V_2O_{11}$ α, β, and γ. Our choice fell on doubly substituted phases by silicon and another element. The latter is chosen from the d (Cu and Co) and p (Si and P) blocks.

The present work is devoted to the structural analysis of the compound $Bi_4V_{1.7}Si_{0.3}O_{10.85}$ (The chemical composition of this compound $Bi_4V_{1.7}Si_{0.3}O_{10.85}$ has been calculated from the general formula $Bi_4V_{2-x}Si_xO_{11-x/2}$ and is a theoretical composition) and the doped series $Bi_4V_{1.7}Si_{0.15}Me_{0.15}O_{11-\delta}$ (Me = Si, P, Cu, and Co) obtained by substituting 15% vanadium (denoted BISIMEVOX.15 or $Bi_4V_{1.7}(Si.Me)_{0.3}O_{11-\delta}$). The main objective is to study the effect of the nature of the dopant on the crystalline structure and on the optical properties.

2. Experimental

Polycrystalline samples of the formula $Bi_4V_{1.7}(Si.Me)_{0.3}O_{11-\delta}$ (Me= Si, P, Cu, and Co) were prepared by conventional solid-state reaction. Stoichiometric amounts of Bi_2O_3 (99.5%), V_2O_5 (99%), SiO_2 (99.9%), $(NH_4)_2HPO_4$ (99%), CuO (99%), and CoO (99%) were ground for 20 minutes, and heated in air at 800 °C for 24 h, then cooled to room temperature (two anneals were necessary to obtain pure products, and 3g of powder was prepared). For the phosphorus-based compound, a pretreatment allowing the release of NH_3 and H_2O was performed at 400 °C for 12 h. X-ray diffraction (XRD) analysis was conducted on the powder samples using a Rigaku SmartLab SE instrument, utilizing CuKα radiation with a wavelength of 1.54059 Å. The measurements spanned a 2θ range from 5 ° to 80 °, with a scanning rate of 2 °/min and a step width of 0.02°. The unit cell parameters were determined using the Rietveld refinement method. The parameter values obtained with the DICVOL06 software are used as a starting model in the Full Prof software. The average crystallite size of the prepared powders was estimated using the Scherrer formula [20]:

$$D = {}^{0.9\,\lambda}/_{\beta cos\theta} \qquad \text{Eq.1}$$

Where D is the average crystallite size in nm, β is the full width at half maximum (FWHM) of the X-ray diffraction peaks, θ is the Bragg angle and λ is the wavelength of Cu-K_α radiation

Raman scattering spectra were recorded for samples in the form of powders, using a Confotec MR520 spectrometer, with a laser emitting in the green at wavelength λ = 532 nm.

The IR spectra were recorded using the KBr pellet technique, in the 4000 to 400 cm^{-1} wavenumber region at room temperature, using a Bruker VERTEX 70 FTIR spectrometer equipped with a DTGS detector and OPUS 6.5 software; 128 scans with 2 cm^{-1} resolution, in transmittance mode.

Analysis of phase transitions with temperature for all samples was performed by differential scanning calorimetry (DSC) measurements in the air using a DSC 131 EVO at a heating rate of 10 °C min^{-1}.

The surface morphology of the sintered ceramics and powders was studied using a scanning electron microscope (VEGA3), equipped with energy-dispersive X-ray spectroscopy (EDS). The measurements were carried out on pellets that had been sintered at a temperature of 830 °C for a duration of 5 hours.

The optical properties of the powdered samples were studied by diffuse reflectance spectroscopy (DRS) at room temperature in the UV-Vis regions in the wavelength range of 200-800 nm using a Shimadzu spectrophotometer (UV-3101).

3. Results and discussion

3.1. Structural characterization

Figure 1 shows the room temperature X-ray diffraction patterns of the prepared samples $Bi_4Si_{0.15}Me_{0.15}V_{1.7}O_{11-\delta}$ (Me = Si, P, Cu, and Co) in the 2θ range 10°- 65 °. Depending on the nature of the substituent ion, the obtained phases are isotypical to either the monoclinic, orthorhombic, or tetragonal polymorph of $Bi_4V_2O_{11}$.

For the single substitution by silicon, the XRD analysis shows that $Bi_4Si_{0.3}V_{1.7}O_{11-\delta}$ is a β-orthorhombic phase with the Amam space group. In the case of the double substitution (Si,P), the diffractogram of the obtained compound $Bi_4Si_{0.15}P_{0.15}V_{1.70}O_{11-\delta}$, reveals the presence of doublets at 2θ= 32, 34, 40, 48, and 55°, as well as a superstructure peak at 2θ ≈ 24.2°, which are characteristic of the α-monoclinic polymorph with the C2/m space group. On the other hand, in the case of double substitution by (Si,Cu) and (Si,Co), the doublet diffraction peaks at 2θ≈32, 34, and 55 ° become singlets which reveal the formation of a γ-tetragonal phase with the space group I4/mmm for the compounds $Bi_4Si_{0.15}Cu_{0.15}V_{1.70}O_{11-\delta}$ and $Bi_4Si_{0.15}Co_{0.15}V_{1.70}O_{11-\delta}$. For all the compounds studied, no diffraction line indicating the presence of a secondary phase was detected.

It should be noted that in the case of the BISIVOX ($Bi_4V_{2-x}Si_xO_{11-\delta}$) solid solution ($0.0 \leq x \leq 0.4$), which we have studied in previous work [21], only the composition x= 0.35 allowed the γ- $Bi_4V_2O_{11}$ form to be obtained. However, in the case of the BISIPVOX ($Bi_4V_{2-x}Si_{x/2}P_{x/2}O_{11-\delta}$) solid solution ($0.0 \leq x \leq 0.5$), we did not obtain any γ-$Bi_4V_2O_{11}$ type phase (only the α and β polymorphs were obtained) [18]. As it has been shown for the compounds BIPVOX ($Bi_4V_{2-x}P_xO_{11}$, $0.0 \leq x \leq 0.2$), the strongly covalent character of the bonds is not favorable to the disorder which characterizes the γ phase [22]. The two compounds $Bi_4V_{1.7}Si_{0.15}Cu_{0.15}O_{11-\delta}$ and $Bi_4V_{1.7}Si_{0.15}Co_{0.15}O_{11-\delta}$ compounds crystallize in the γ-form as was the case with $Bi_4V_{1.7}(Al.Cu)_{0.3}O_{11-\delta}$ synthesized by Essalim et *al*. [10].

In summary, it can be seen that phosphorus doping of the compound with theoretical formula $Bi_4Si_{0.3}V_{1.7}O_{10.85}$, accompanied by a decrease in the rate of oxygen vacancies on the one hand and an increase in the covalence of the M-O bond on the other hand, leads to the transition to a less symmetrical structure (from β-$Bi_4Si_{0.3}V_{1.7}O_{10.85}\square_{1.15}$ to α-$Bi_4Si_{0.15}P_{0.15}V_{1.70}O_{10,925}\square_{1.075}$) (decreased disorder). It can be noted that the double substitution by (P, Si) nevertheless leads to obtaining a solid solution existing over a wider composition range with $x > x_{max}$ of BIPVOX solid solution ($x_{max} = 0.2$). However, Cu and Co, being weakly charged and of medium sizes, the M-O bonds are not very covalent, we also see that the doping of $Bi_4Si_{0.3}V_{1.7}O_{10.85}$ by Cu or by Co leads to an increase in the rate of oxygen vacancies (Vacant oxygen quantities are theoretical). These two parameters are favorable to the creation of disorder in the network. Thus, in both cases, we observe the transition to a more symmetrical structure (from β-$Bi_4Si_{0.3}V_{1.7}O_{10.85}\square_{1.15}$ to γ-$Bi_4Si_{0.15}Cu_{0.15}V_{1.70}O_{10,70}\square_{1.30}$ and γ-$Bi_4Si_{0.15}Co_{0.15}V_{1.70}O_{10,70}\square_{1.30}$).

The variation of the lattice parameters of BISIMEVOX.15 (Me = Si, P, Cu, and Co) is presented in Table 1**.** To allow comparison, all lattice parameters were related to the dimensions of the average cell. Thus, without taking into account the nature of the polymorph, we compare the values of the cell parameters of the four compounds. We find that the a parameter varies weakly ($\Delta a/a \approx 0.3\%$) compared to the c parameter ($\Delta c/c \approx 1.3\%$), showing that the crystal structure has a pronounced two-dimensional character. Furthermore, we found, when studying several BIMEVOX [18, 19, 23, 24] that the parameter a depends little on the size of the dopant ion and is rather sensitive to the covalent character of the Me-O bond and the rate of anionic vacancies in the perovskite layers (the vacancies are preferentially located in equatorial positions). Considering the difference in the ionic radii and the charge of the cations, we can make a qualitative comparison of their polarizing powers and therefore we can qualitatively compare the covalence of the bonds. Thus, the compound BISIPVOX presents the lowest value of the parameter a because of the strong covalent character of the ME-O bond**.** While the other three BISIMEVOX.15 compounds: $Bi_4V_{1.7}Si_{0.3}O_{10.85}$, $Bi_4V_{1.7}(Si.Cu)_{0.3}O_{10.7}$ and $Bi_4V_{1.7}(Si.Co)_{0.3}O_{10.7}$), which have almost the same ratio of anionic vacancies, have almost the same value of parameter ***a*** despite the difference in the size of the doping element ME. However, the ***c*** parameter varies in the same direction as the ionic radius of ME (ionic radii: $r_i(P^{5+}) = 0.38$ Å $r_i(Si^{4+}) = 0.40$ Å, $r_i(Cu^{2+}) = 0.73$ Å and $r_i(Co^{2+}) = 0.74$ Å [25]).

The values of the average crystallite size (D) were calculated from the Scherrer formula and are given in Table 1. The average size increases from the monoclinic α-phase to the orthorhombic β-phase and then to the tetragonal γ-phase, as the number of vacancies increases which facilitates the diffusion of ions in the lattice and promotes crystal growth [26].

3.2. FTIR and Raman analysis

Figure 2 shows the FT-IR spectra of the BISIMEVOX.15 compounds. The band around 510-525 cm^{-1} is mainly attributed to the stretching vibration of the Bi-O bond in the octahedral units of BiO_6 [10, 27]. The absorption bands in the 710-730 and 800-890 cm^{-1} regions are attributed to the symmetric ν_s(V-O), and asymmetric ν_{as}(V-O) stretching vibration modes in the vanadate layers, respectively. It should be noted that the position of the latter band varies according to the nature of the dopant element ME, reflecting the variation of the V-O bond length under the effect of doping. Indeed, P^{5+} doping seems to create deformations leading to a decrease in the length of the V-O bond, which results in the displacement of the band from 815 cm^{-1} for BISIVOX.15 ($Bi_4V_{1.7}Si_{0.3}O_{10.85}$) to 824 cm^{-1} for BISIPVOX.15 ($Bi_4V_{1.7}(Si.P)_{0.3}O_{10.7}$). Furthermore, we note the band located at 620 cm^{-1} for the α-monoclinic phase BISIPVOX.15 disappears completely from the IR spectrum of the β-orthorhombic phase BISIVOX and the γ-tetragonal phases BISICUVOX.15 ($Bi_4V_{1.7}(Si.Cu)_{0.3}O_{10.7}$) and BISICOVOX.15 ($Bi_4V_{1.7}(Si.Co)_{0.3}O_{10.7}$), this seems to indicate the banning of some vibrational modes following a change in local symmetry. For the compounds BISICUVOX.15 and BISICOVOX.15, we note the appearance of two bands around 452 and 424 cm^{-1} which can be attributed to the metal dopant-oxygen bond (Cu-O) and (Co-O) [16, 27]. Thus, in agreement with the results of the XRD analysis, the FT-IR spectroscopy study highlights modifications of the local symmetry and bond strength according to the nature of the doping ion.

Room temperature Raman spectra for the compounds BISICUVOX.15, BISIVOX.15, and BISIPVOX are presented in Figure 3.

Similar to our previous studies on BIMEVOX [18, 19], there are two strong signal regions in the high frequency (600-940 cm^{-1}) and low frequency (130-450 cm^{-1}) regions. The high-frequency region is mainly associated with the stretching vibrations of the V-O bond in vanadium polyhedra. The signal at 930 and 918 cm^{-1}, as observed in BISIPVOX.15 and BISIVOX.15 spectra, respectively, gradually shifts to lower frequencies and merges with the main peak at the α→β transition. This peak is attributed to the stretching of the V-O bond in a V-O-V chain structure. The existence of such chains was observed in the α and β phases during a structural study as a function of the temperature of $Bi_4V_2O_{11}$ carried out by Patwe et *al* [28]. These chains disappear during the transition to the γ form. The low-frequency signals (130-260 cm^{-1}) are mainly associated with external modes corresponding to chain bending. The remaining signals between 360- 380 cm^{-1} are associated with V-O bending vibration modes. The band located at about 530 cm^{-1}, corresponds to the symmetric stretching mode of the V-O bond, while the signals located at 600-860 cm^{-1} are assigned to the asymmetric stretching mode of the V-O bond [29, 30]. The strong mode observed in the region of 845-860 cm^{-1} is due to the symmetric stretching modes of the V-O band of VO_4 groups [31]. Note that the band corresponding to this mode,

located for BISIVOX.15 at 847 cm^{-1}, gradually shifted to 855 cm^{-1} and 852 cm^{-1} for the compounds BISIPVOX.15 and BISICUVOX.15, respectively. From the positions of these bands, we calculated the corresponding V-O bond length using the empirical formula proposed by Hardcastle et *al* [32] (Equation 2):

$$\nu = 21349 \times \exp(-1.9176 \times R) \qquad \text{Eq (2)}$$

(ν is the vibration band frequency and R is the length of the V-O bond). This equation was established with the diatomic approximation where each vanadium-oxygen bond vibrates independently of the crystal lattice. The values obtained are 1.6828 Å, 1.6797 Å, and 1.6779 Å for BISIVOX.15, BISICUVOX.15, and BISIPVOX.15, respectively. These values show that changes in the local environment of vanadium are induced by doping with elements of different natures. We also note that the shortest bond is obtained in the case of doping by phosphorus, which is in agreement with the lowest values of the lattice parameters obtained by the XRD analysis. We can conclude that the study by Raman spectroscopy has shown, in agreement with the results of FT-IR spectroscopy and those of XRD, that depending on the nature of the doping element, structural changes and modifications of the local symmetry have been well confirmed.

3.3. DSC analysis and SEM micrographs

The DSC thermograms of the compound BISIMEVOX.15 from 50 °C to 550 °C are shown in Figure 4. The DSC curve of the α-monoclinic phase BISIPVOX shows two endothermic peaks appeared upon heating at 453 °C and 489 °C, attributed to α→β and β→γ phase transitions, respectively (these transitions are not accompanied by a gain or loss of mass). The BISIVOX.15 compound shows a single endothermic peak at 425 °C, attributed to the β→γ transition. In the case of the BISICUVOX.15 sample, no thermal phenomena were recorded, indicating the stabilization of the γ-tetragonal polymorph at room temperature. Upon cooling, all phenomena recorded during the temperature rise are observed at almost the same temperatures, showing the reversibility of the local transformations. These results are in good agreement with the results of the XRD analysis.

Figure 5 shows SEM micrographs of ceramics sintered at 830 °C for 5h and synthesis powder (in the inset of the figure) for all BISIMEVOX.15 samples (Me = Si, P, Cu, and Co). Note first that the morphology of the synthesized powders BISIMEVOX.15 is almost independent of the nature of the doping ion and that the grain size varies from 10 to 30 μm. Nevertheless, the microstructure of sintered samples is strongly dependent on the doping element. The Si^{IV}-P^{V} doped ceramic shows a large grain size of about 25 μm, and some microcracks are also observed. This can be explained by the decrease in melting point in the presence of phosphorus [18, 22], and consequently, excessive grain growth leads to the appearance of microcracks. Si^{IV}, Si^{IV}-Cu^{II}, and Si^{IV}-Co^{II} doped ceramics show well-defined

grains separated by visible grain boundaries. Moreover, intergranular pores are observed for the Si^{IV}-Co^{II} doped sample. One can also observe, for this sample, relatively darker spots which indicate the presence of a secondary phase less rich in bismuth or a phase of the V-Me system as seen in other works [33].

EDX analysis was performed for the ceramics and the results are presented in Table 2. The identified elements are: Bi, V, Si, P, Cu, Co, and O. Overall, the experimental atomic percentages (% exp) agree with the stoichiometry of the synthesized compounds (% theo).

3.4. UV–Visible spectroscopy measurements

The optical absorption properties of semiconductors associated with the electronic structure play an essential role in photo-catalytic activity [34, 35].

Figure 6 shows the diffuse reflectance spectra (DRS) of BISIMEVOX.15 in the 250-800 wavelength range. The direct band gaps (Eg) of the prepared compounds were obtained by plotting $F(R)\ h\nu)^2$ as a function of $h\nu$ (1240/λ (nm)) and then extrapolating the linear portion of the graph to the x-axis, as shown in Figure 7. The results of the band gap determination are given in Table 3. The band shape of the studied compounds is similar to that of $Bi_4V_2O_{11}$ [15, 36], except for the compound BISICOVOX.15, where an additional fuzzy reflection minimum is observed. This minimum can be explained by the existence of electron transfers that correspond to the absorption of emission in cobalt polyhedra characteristic of the BICOVOX structure [37, 38]. On the other hand, the compound BISIPVOX.15, BISIVOX.15, BISICUVOX.15 and BISICOVOX.15 show absorption in visible light with an absorption edge at 525.7, 551.5, 579.8, and 705 nm, respectively.

As shown in Figure 7, the band gap energies Eg of BISIPVOX.15, BISIVOX.15, BISICUVOX.15, and BISICOVOX.15 were estimated to be 2.36 eV, 2.25 eV, 2.14 eV, and 1.76 eV, respectively. It should be noted that the experimental values of Eg are different, due to the difference in phase symmetry and the doping element ME. The smaller optical band gap energy is obtained for BISICOVOX.15. This is undoubtedly attributed to the additional contribution of Co3d orbitals to the conduction band and the increased concentration of oxygen vacancies in the vanadate layers [39]. Globally, the values of band gap energy Eg are lower than that of $Bi_4V_2O_{11}$(2.46 eV) [17], and $BiVO_4$ (2.4 eV) [40]. Moreover, The estimated E_g values obtained by K. Trzciński et al. [17], for the orthorhombic α-$Bi_4V_2O_{11}$ and for compounds with substitution rate x = 0.2 in BICUVOX ($Bi_4V_{2-x}Cu_xO_{11-\delta}$) (γ-form), BIZNVOX ($Bi_4V_{2-x}Zn_xO_{11-\delta}$) (α-form), and BIMNVOX ($Bi_4V_{2-x}Mn_xO_{11-\delta}$) (γ -form) systems, are 2.46, 2.34, 2.27 and 2.18 eV, respectively. It is clear that the Eg values obtained for our samples are not very different from those obtained for the monosubstituted phases studied by K. Trzciński. However, the bisubstituted γ-BISICOVOX.15 compound has a significantly lower Eg value, 1.76 eV. Thus,

the double substitution (Si, ME) of vanadium in $Bi_4V_2O_{11}$ made it possible to lower the energy of the gap, which may be favorable to the improvement of the photocatalytic activity in the visible light of the obtained compounds.

4. Conclusion

In this work, the series of BISIMEVOX.15 compounds, $Bi_4V_{1.7}(Si.Me)_{0.3}O_{11-\delta}$ (Me= Si, P, Cu, and Co), was obtained by coupled substitution of 15% vanadium with Si and Me in $Bi_4V_2O_{11}$. XRD showed that the three polymorphs of BIMEVOX, α, β, and γ, are stabilized at room temperature for ME = P, Si, and Cu/Co, respectively. The obtaining of these polymorphs was confirmed and local deformations were highlighted by Raman and FT-IR spectroscopies in relation to the nature of the doping element. DSC showed two reversible phase transitions $\alpha\leftrightarrow\beta$ and $\beta\leftrightarrow\gamma$ for $Bi_4V_{1.7}(Si.P)_{0.3}O_{11-\delta}$, a single reversible transition $\beta\leftrightarrow\gamma$ for $Bi_4V_{1.7}Si_{0.3}O_{11-\delta}$, and no transition for the tetragonal phases $Bi_4V_{1.7}(Si.Cu)_{0.3}O_{11-\delta}$ and $Bi_4V_{1.7}(Si.Co)_{0.3}O_{11-\delta}$. The DRS spectra reveal that the band gap energy values of the double-doped BISIMEVOX.15 compounds ($1.76 \leq Eg \leq 2.36$ eV) are lower than some values encountered in the literature for the parent compound $Bi_4V_2O_{11}$. The band gap reduction can be explained by generated local defects that improve the optical properties of $Bi_4V_2O_{11}$.

Declaration of competing interest

The authors declare no conflicts of interest.

Ethical Approval

Not applicable.

Competing interests

Not applicable.

Author Contributions

A. AGNAOU: investigation, writing original draft, formal analysis; W. MHAIRA: helped the interpretation of results; R. ESSALIM: writing review and editing; M. ALGA: investigation; M. ZAMAMA: investigation; F. MAUVY: investigation; A. AMMAR: conceived the idea and supervision.

Funding

Not applicable.

Availability of data and materials

Not applicable.

Acknowledgments

The authors are grateful to the Cadi Ayyad University Analysis and Characterization Center (CAC) for providing them with materials characterization techniques.

References

1. Abraham F, Debreuille-Gresse MF, Mairesse G, Nowogrocki G (1988) Phase transitions and ionic conductivity in $Bi_4V_2O_{11}$ an oxide with a layered structure. Solid State Ionics 28–30:529–532. https://doi.org/10.1016/S0167-2738(88)80096-1
2. Boivin J (1998) Electrode-electrolyte BIMEVOX system for moderate temperature oxygen separation. Solid State Ionics 113–115:639–651. https://doi.org/10.1016/S0167-2738(98)00330-0
3. Pirovano C, Vannier RN, Nowogrocki G, et al (2003) Characterisation of the electrode-electrolyte BIMEVOX system for oxygen separation: Part II. Thermal studies under controlled atmosphere. Solid State Ionics 159:181–191. https://doi.org/10.1016/S0167-2738(03)00078-X
4. Lacorre P, Goutenoire F, Bohnke O, et al (2000) Designing fast oxide-ion conductors based on $La_2Mo_2O_9$. Nature 404:856–858. https://doi.org/10.1038/35009069
5. Iharada T, Hammouche A, Fouletier J, et al (1991) Electrochemical characterization of BIMEVOX oxide-ion conductors. Solid State Ionics 48:257–265. https://doi.org/10.1016/0167-2738(91)90040-I
6. Abraham F, Boivin J, Mairesse G, Nowogrocki G (1990) The BIMEVOX series: A new family of high performances oxide ion conductors. Solid State Ionics 40–41:934–937. https://doi.org/10.1016/0167-2738(90)90157-M
7. Abrahams I (2003) A model for the mechanism of low temperature ionic conduction in divalent-substituted γ-BIMEVOXes. Solid State Ionics 157:139–145. https://doi.org/10.1016/S0167-2738(02)00201-1
8. Mairesse G, Roussel P, Vannier RN, et al (2003) Crystal structure determination of α, β and γ- $Bi_4V_2O_{11}$ polymorphs. Part I: γ and β- $Bi_4V_2O_{11}$. Solid State Sci 5:851–859. https://doi.org/10.1016/S1293-2558(03)00015-3
9. Mairesse G, Roussel P, Vannier RN, et al (2003) Crystal structure determination of α-, β- and γ- $Bi_4V_2O_{11}$ polymorphs. Part II: crystal structure of α- $Bi_4V_2O_{11}$. Solid State Sci 5:861–869. https://doi.org/10.1016/S1293-2558(03)00016-5
10. Essalim R, Ammar A, Zamama M, Mauvy F (2020) A study on structural properties, conductivity and FT-IR spectroscopy of Cu–Al doubly substituted $Bi_4V_2O_{11}$. J Solid State Chem 288:121405. https://doi.org/10.1016/j.jssc.2020.121405
11. Abrahams I, Krok F, Malys M, Wrobel W (2005) Phase transition studies in BIMEVOX solid electrolytes using AC impedance spectroscopy. Solid State Ionics 176:2053–2058. https://doi.org/10.1016/j.ssi.2004.08.044
12. Pasciak G, Prociow K, Mielcarek W, et al (2001) Solid electrolytes for gas sensors and

fuel cells applications. J Eur Ceram Soc 21:1867–1870. https://doi.org/10.1016/S0955-2219(01)00132-7

13. Anwar K, Naqvi FK, Beg S, Haneef S (2023) Photocatalytic degradation of MB dye and paracetamol drug, via hydrothermally synthesised praseodymium doped $Bi_4V_2O_{11}$ nanoparticles. J Mol Struct 1272:134183. https://doi.org/10.1016/j.molstruc.2022.134183
14. Lu Y, Pu Y, Wang J, et al (2015) On structure and methylene blue degradation activity of an Aurivillius-type photocatalyst of $Bi_4V_2O_{11}$ nanoparticles. Appl Surf Sci 347:719–726. https://doi.org/10.1016/j.apsusc.2015.04.164
15. Tripathy D, Saikia A, Tado GT, Pandey A (2019) Role of Al and Ti doping in modulating electrical properties of BIMEVOX system. J Adv Ceram 8:489–499. https://doi.org/10.1007/s40145-019-0329-1
16. Al-Areqi N, Umair M, Senan A, et al (2022) Mesoporous Nano-Sized BiFeVOx.y Phases for Removal of Organic Dyes from Wastewaters by Visible Light Photocatalytic Degradation. Nanomaterials 12:1383. https://doi.org/10.3390/nano12081383
17. Trzciński K, Borowska-Centkowska A, Sawczak M, Lisowska-Oleksiak A (2015) Photoelectrochemical properties of BIMEVOX (ME = Cu, Zn, Mn) electrodes in contact with aqueous electrolyte. Solid State Ionics 271:63–68. https://doi.org/10.1016/j.ssi.2014.10.008
18. Agnaou A, Mhaira W, Essalim R, et al (2023) Structural study and ionic conductivity of $Bi_4V_{2-x}Si_{x/2}P_{x/2}O_{11-\delta}$ ($0.0 \leq x \leq 0.5$) compounds. J Solid State Chem 318:123730. https://doi.org/10.1016/j.jssc.2022.123730
19. Mhaira W, Agnaou A, Essalim R, et al (2023) Effect of simultaneous Cu and Nb doping $Bi_4V_2O_{11}$ on structural and electrical properties of $Bi_4V_{2-x}Cu_{x/2}Nb_{x/2}O_{11-3x/4}$. J Solid State Chem 320:123878. https://doi.org/10.1016/j.jssc.2023.123878
20. Scherrer P (1912) Bestimmung der inneren Struktur und der Größe von Kolloidteilchen mittels Röntgenstrahlen. In: Kolloidchemie Ein Lehrbuch. Springer Berlin Heidelberg, Berlin, Heidelberg, pp 387–409
21. Agnaou A, Mhaira W, Essalim R, et al (2023) Correction: New silicon substituted BiMeVO x : synthesis and study of structural properties in relation to ionic conductivity. RSC Adv 13:8943–8943. https://doi.org/10.1039/D3RA90021E
22. Alga M, Ammar A, Essalim R, et al (2005) Synthesis, sintering and electrical properties of P-doped $Bi_4V_2O_{11}$ ceramics. Solid State Sci 7:1173–1179. https://doi.org/10.1016/j.solidstatesciences.2005.06.011
23. Essalim R, Tanouti B, Bonnet J-P, Réau JM (1992) Elaboration and electrical properties of ($0.20 \leqslant x \leqslant 0.55$) ceramics with the Y-$Bi_4V_2O_{11}$ type structure. Mater Lett 13:382–386. https://doi.org/10.1016/0167-577X(92)90073-S

24. Essalim R, Ammar A, Tanouti B, Mauvy F, (2016) Synthesis, thermal and electrical properties of Al-doped $Bi_4V_{1.8}Cu_{0.2}O_{10.7}$. J Solid State Chem 240:122–125. https://doi.org/10.1016/j.jssc.2016.05.026
25. Shannon RD (1976) Revised effective ionic radii and systematic studies of interatomic distances in halides and chalcogenides. Acta Crystallogr Sect A 32:751–767. https://doi.org/10.1107/S0567739476001551
26. Tripathy D, Saikia A, Tado GT, Pandey A (2018) Dielectric study of Ti-doped $Bi_2VO_{5.5}$ solid electrolyte. Indian J Phys 93:845–859. https://doi.org/10.1007/s12648-018-1356-4
27. Sharma S, Yashwanth PK, Roy B (2021) Deactivation study of the BICOVOX catalysts used in low temperature steam reforming of ethanol for H2 production. J Phys Chem Solids 156:110138. https://doi.org/10.1016/j.jpcs.2021.110138
28. Patwe SJ, Patra A, Dey R, et al (2013) Probing the Local Structure and Phase Transitions of Bi 4 V 2 O 11 -Based Fast Ionic Conductors by Combined Raman and XRD Studies. J Am Ceram Soc 96:3448–3456. https://doi.org/10.1111/jace.12490
29. Yue Y, Dzięgielewska A, Krok F, et al (2022) Local Structure and Conductivity in the BIGAVOX System. J Phys Chem C 126:2108–2120. https://doi.org/10.1021/acs.jpcc.1c08825
30. Yue Y, Dzięgielewska A, Hull S, et al (2022) Local structure in a tetravalent-substituent BIMEVOX system: BIGEVOX. J Mater Chem A 10:3793–3807. https://doi.org/10.1039/D1TA07547K
31. Joubert O, Jouanneaux A, Ganne M (1994) Crystal structure of low-temperature form of bismuth vanadium oxide determined by rietveld refinement of X-ray and neutron diffraction data (α-$Bi_4V_2O_{11}$). Mater Res Bull 29:175–184. https://doi.org/10.1016/0025-5408(94)90138-4
32. Hardcastle FD, Wachs IE (1991) Determination of vanadium-oxygen bond distances and bond orders by Raman spectroscopy. J Phys Chem 95:5031–5041. https://doi.org/10.1021/j100166a025
33. Lazure S, Vannier RN, Nowogrocki G, et al (1995) BICOVOX family of oxide anion conductors: Chemical, electrical and structural studies. J Mater Chem 5:1395–1403. https://doi.org/10.1039/jm9950501395
34. Zhao X, Duan Z, Chen L (2019) Bi-Quantum-Dot-Decorated $Bi_4V_2O_{11}$ Hollow Nanocakes: Synthesis, Characterization, and Application as Photocatalysts for CO 2 Reduction. Ind Eng Chem Res 58:10402–10409. https://doi.org/10.1021/acs.iecr.9b01737
35. Li J, Lu P, Deng W, et al (2020) Facile synthesis of sheet-like $BiVO_4$/$Bi_4V_2O_{11}$ composite for enhanced photocatalytic properties. Mater Chem Phys 123489. https://doi.org/10.1016/j.matchemphys.2020.123489

36. Liang M, Yang Z, Mei Y, et al (2018) Dye-Sensitized-Assisted, Enhanced Photocatalytic Activity of $TiO_2/Bi_4V_2O_{11}$. Nano 13:1850028. https://doi.org/10.1142/S1793292018500285
37. Al-Areqi NAS, Beg S, Al-Alas A, Hafeez S (2013) Stabilized γ-BIMNVOX solid electrolyte: Ethylene glycol–citrate sol–gel synthesis, microwave-assisted calcination, and structural and electrical characterization. J Alloys Compd 581:79–85. https://doi.org/10.1016/j.jallcom.2013.07.038
38. Buyanova ES, Michaylovkaya ZA, Yurchenko M V., Lipina OA (2020) Photocatalytic Characteristics of Complex Oxides $Bi_4V_{1.8}Me_{0.2}O_{11-\delta}$ (Me = Co, Cu, Fe, Mn, Nb). Russ J Phys Chem A 94:2527–2533. https://doi.org/10.1134/S0036024420120067
39. Al-Areqi NAS, Al-Kamali ASN, Ghaleb KAS, et al (2014) Influence of phase stabilization and perovskite vanadate oxygen vacancies of the BINIVOX catalyst on photocatalytic degradation of azo dye under visible light irradiation. Radiat Eff Defects Solids 169:117–128. https://doi.org/10.1080/10420150.2013.848448
40. Lin Y, Lu C, Wei C (2019) Microstructure and photocatalytic performance of $BiVO_4$ prepared by hydrothermal method. J Alloys Compd 781:56–63. https://doi.org/10.1016/j.jallcom.2018.12.071

Table.1 Unit cell parameters of BISIMEVOX.15 (ME = Si, P, Cu, and Co), and the average crystallite size (D).

BIMEVOX	a (Å)	b (Å)	c (Å)	V(Å^3)	Phase	β (°)	D (nm)	
$Bi_4V_{1.7}(Si.P)_{0.3}O_{11-\delta}$	5.545(1)	5.601(5)	15.247(2)	473.590(8)	α	89.91(3)	63.0	[18]
$Bi_4V_{1.7}Si_{0.3}O_{11-\delta}$	5.562(8)	5.591(7)	15.304(9)	476.066(7)	β	90	70.4	This work
$Bi_4V_{1.7}(Si.Cu)_{0.3}O_{11-\delta}$	5.563(6)	—	15.426(9)	477.518(7)	γ	90	98.6	This work
$Bi_4V_{1.7}(Si.Co)_{0.3}O_{11-\delta}$	5.560(3)	—	15.441(4)	477.400(8)	γ	90	105.9	This work

Table.2 Elemental EDS analysis of BISIMEVOX.15 ceramics (atom %)

Element	**BISIVOX.15**		**BISIPVOX.15**		**BISICUVOX.15**		**BISICOVOX.15**	
	% exp	**% theo**	**% exp**	**% theo**	**% exp**	**% theo**	**% exp**	**% theo**
Bi	21.57	23.73	23.60	23.63	22.88	23.95	23.25	23.95
V	6.68	10.09	8.33	10.04	7.98	10.18	7.79	10.18
O	69.66	64.39	66.02	64.55	67.26	64.07	66.94	64.07
Si	2.06	1.78	1.08	0.88	1.11	0.89	1.17	0.89
P/Cu/Co	—	—	0.97	0.88	0.73	0.89	0.83	0.89

Table.3 Direct band gap of BISIMEVOX.15 compounds

	BISIPVOX.15	**BISIVOX.15**	**BISICUVOX.15**	**BISICOVOX.15**
E_g (eV)	2.36	2.25	2.14	1.76

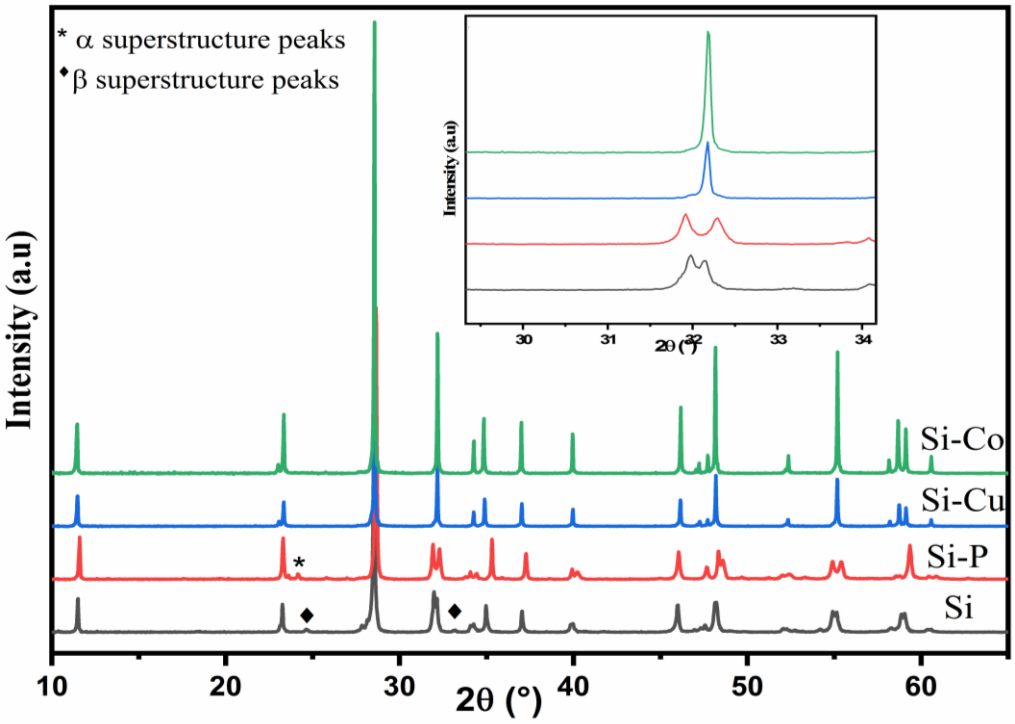

Fig.1 X-ray diffraction patterns of $Bi_4(Si.Me)_{0.3}V_{1.7}O_{11-\delta}$ (Me= Si, P, Cu and Co)

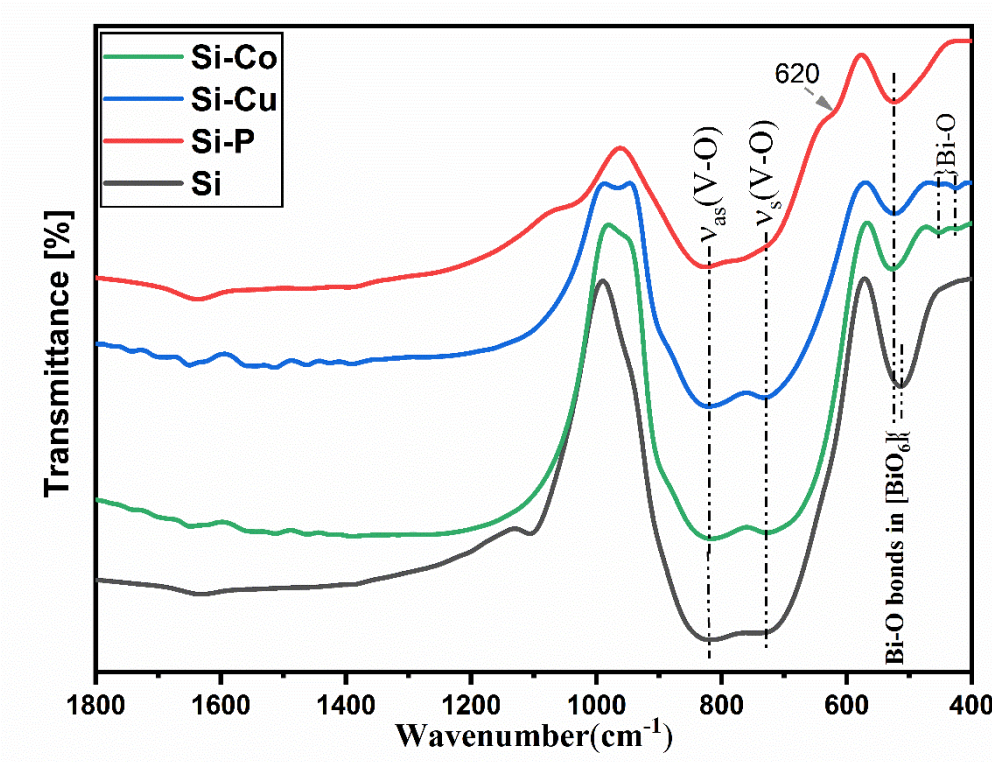

Fig.2 FT-IR spectra of the compound $Bi_4V_{1.7}(Si.Me)_{0.3}O_{11-\delta}$ (Me= Si, P, Cu and Co).

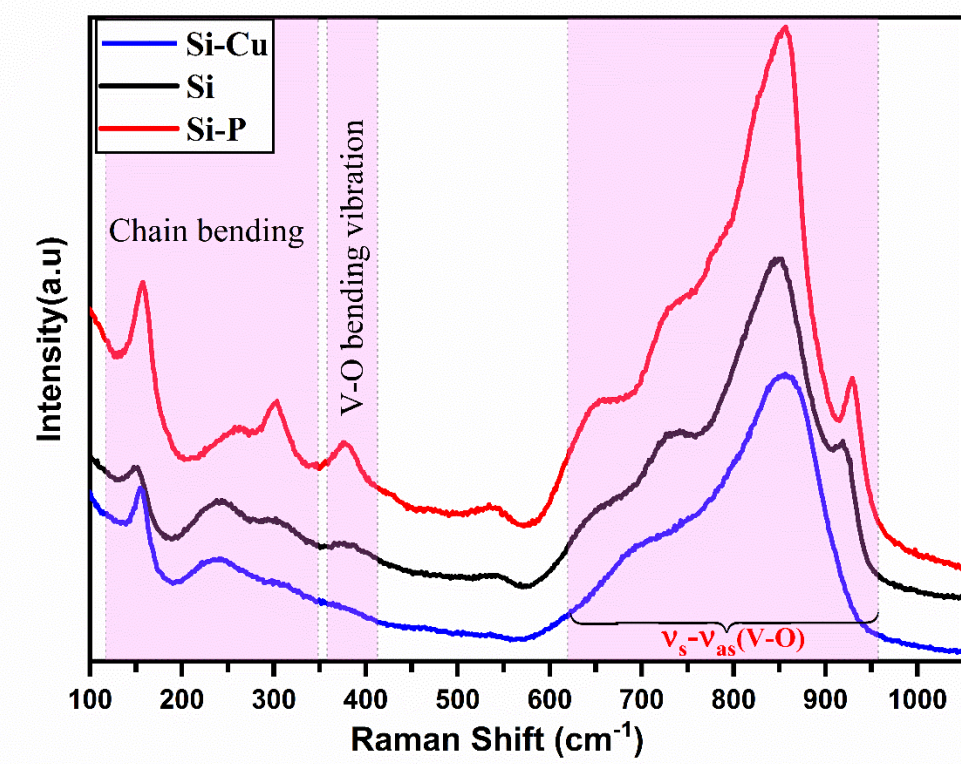

Fig.3 Raman spectra at room temperature for BISIMEVOX.15 compounds

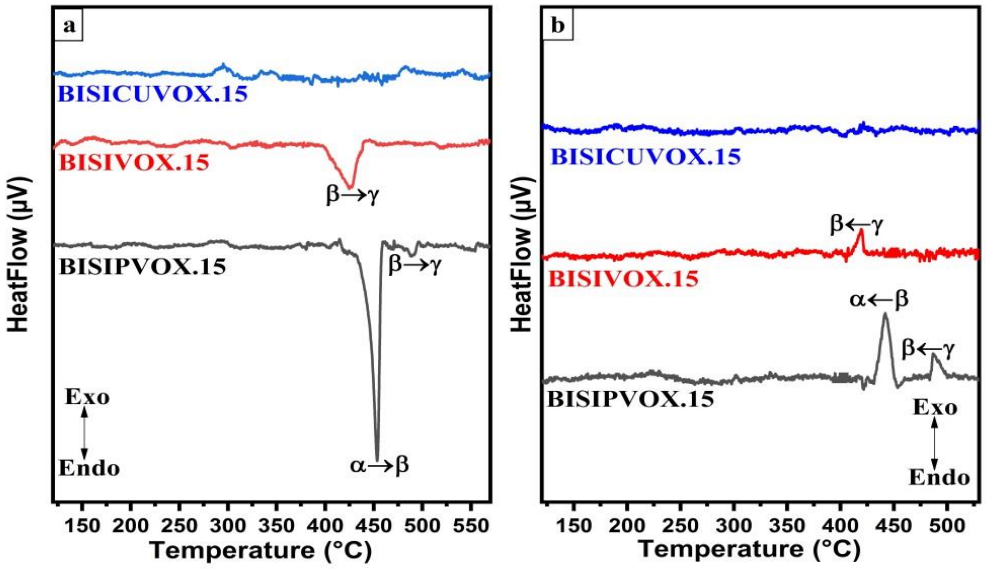

Fig.4 DSC thermo-grams of BISIMEVOX.15 (Me= Si, P, and Cu): a) heating and b) cooling

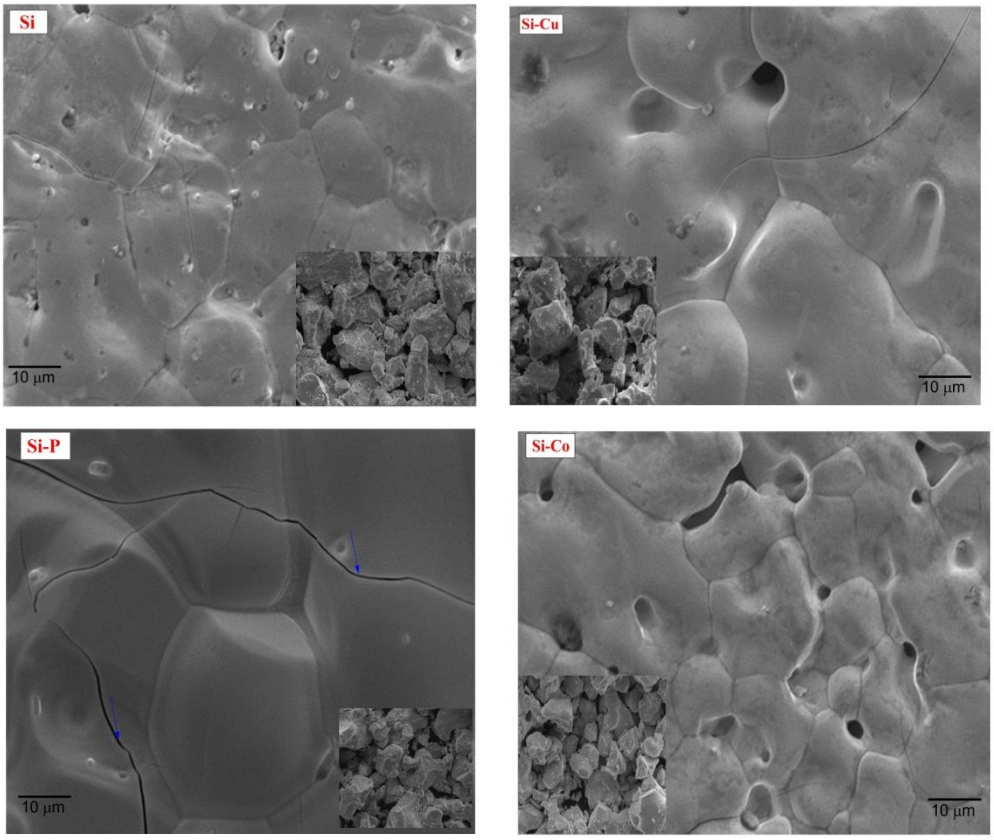

Fig.5 SEM micrographs of BISIMEVOX.15 ceramics and powders (sans in the inset)

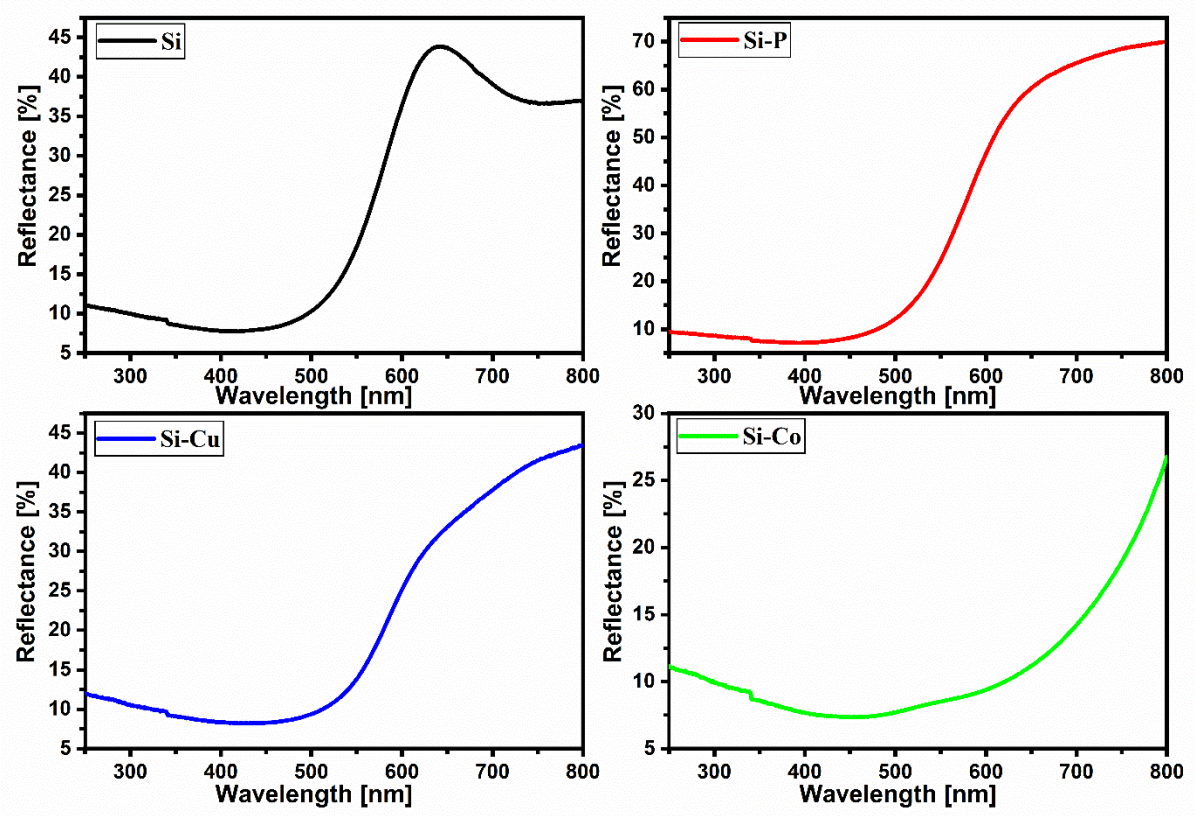

Fig.6 UV–Vis spectra of BISIMEVOX.15

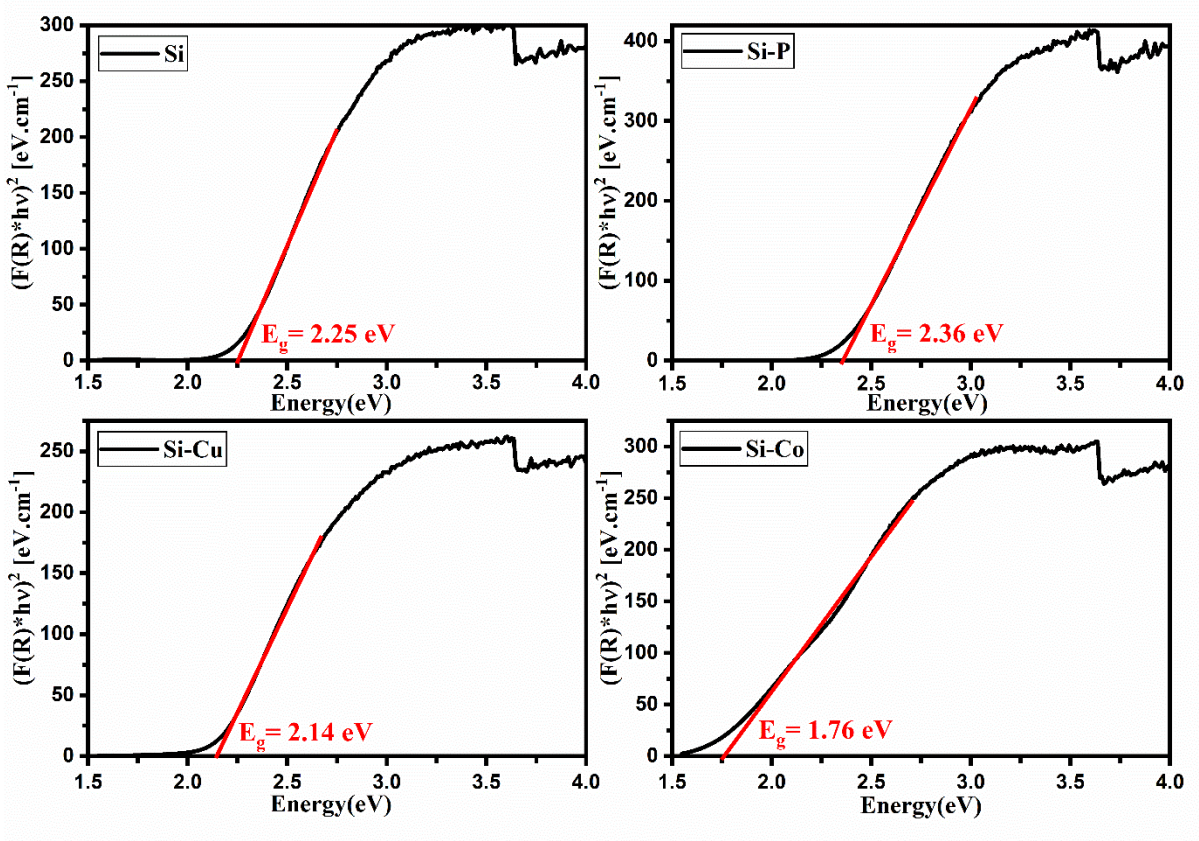

Fig.7 Curves of $(F(R)*h\nu)^2$ versus energy for BISIMEVOX.15.